Slip behavior of velocity-weakening barriers

Diego Molina-Ormazabal [1,2], Jean-Paul Ampuero [3], Andrés Tassara [1,2]

1 Departamento Ciencias de la Tierra, Facultad de Ciencias Químicas, Universidad de Concepción, Concepción, Chile,
2 Millennium Nucleus The Seismic Cycle Along Subduction Zones CYCLO, Valdivia, Chile,
3 Université Côte d'Azur, IRD, CNRS, Observatoire de la Côte d'Azur, Géoazur, Sophia Antipolis, France,

Figures Extended data

Contents

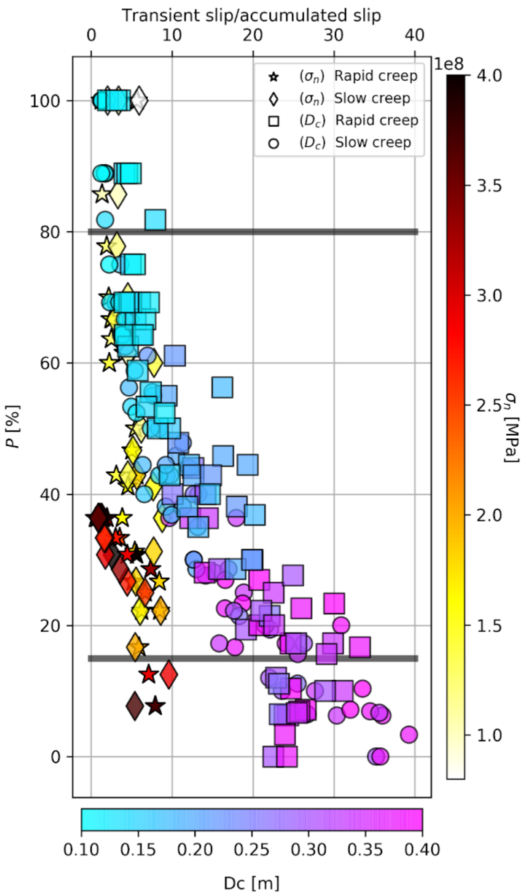

Figure Extended data 1: The diversity of slip behavior in VW barrier types. P as a function of the percentage of rapid creep slip (stars and squares) and slow creep slip (crosses and circles) relative to the total accumulated slip **(see Methods A6)**. A large transient slip relative to the total accumulated slip means an increase in the amount of aseismic slip hosted by the CVWP (x-axis). As Dc is increased (violet colors), the aseismic slip increases too. The same is observed in simulation with normal stress contrast (with values up to twice the asperity σ_n), but when σ_n exceeds twice the asperities' value (red colors), the transient slip decreases, implying an increment in the seismic slip within the CVWP. Further, a smaller ratio between transient and total accumulated slip means major seismic slip within the CCVWP. Warm and cool colors depict variations in σ_n and D_c values respectively whereas vertical gray solid lines display barrier type depending on probability **P**.

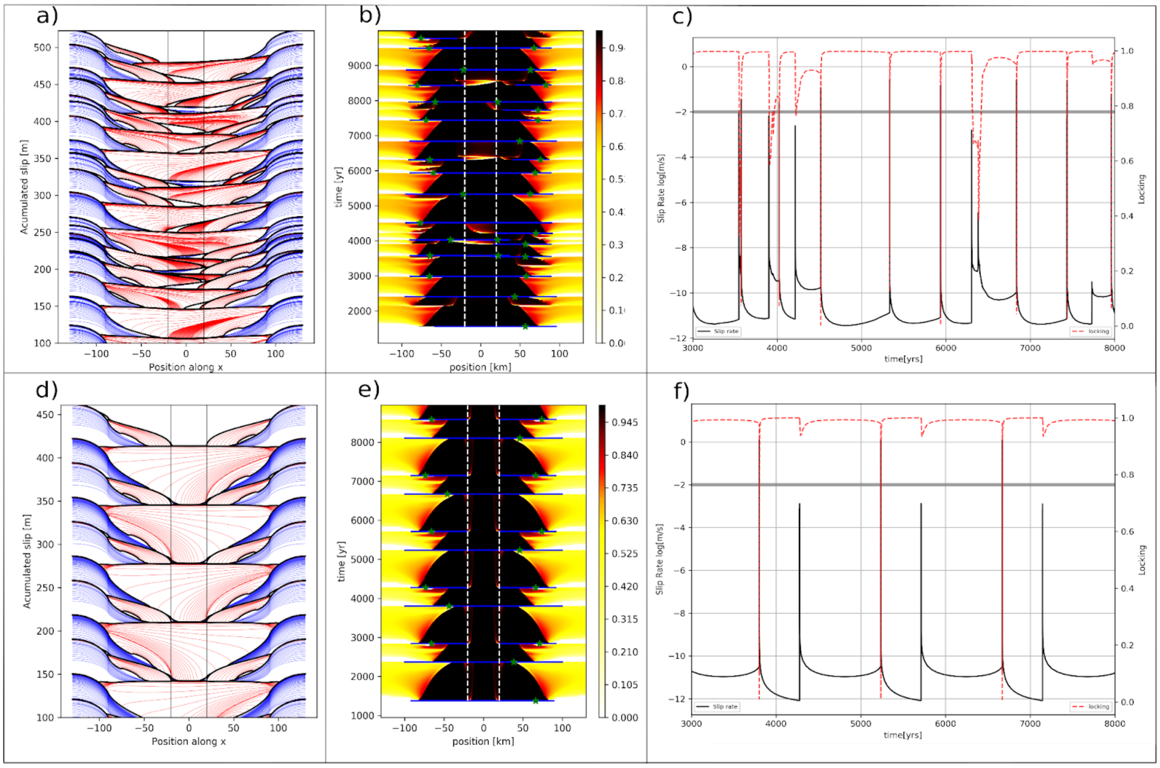

Figure Extended data 2: Seismic cycle simulations of frequent barriers. The barrier has a length of 40 km and is defined by (top) a low $D_c = 0.18\ m$ and (bottom) a high $\sigma_n = 370\ MPa$. a,d): Accumulated slip profiles along the fault during interseismic periods (blue, every 2 years) and during earthquakes (red, every 5 seconds); Black lines depict the start and ending of earthquakes. Solid black lines display the edges of the CVWP. b,e): space-time distribution of instantaneous ISC **(equation 20, see Methods A7).** Blue solid lines and green stars show the rupture length and epicenter of earthquakes, respectively. Dashed white lines indicate the edges of the CVWP. c,f): Instantaneous ISC averaged across the CVWP (red dashed lines) and slip rate averaged across the whole fault (black solid lines) as a function of time. The horizontal gray line indicates our chosen threshold for seismic slip rates, 1 cm/s. ISC varies throughout the seismic cycle, although the values are most often close to 1 (fully locked). Some transients are aseismic, their slip rates do not reach seismic velocities.

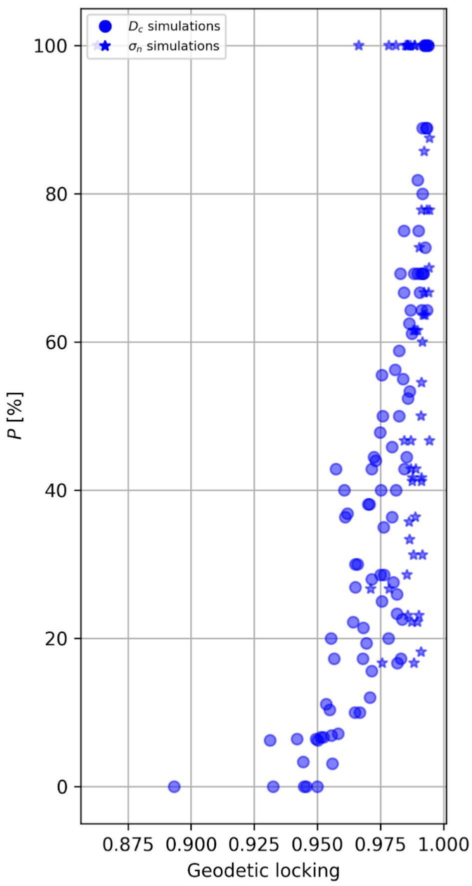

Figure Extended data 3: Long-term interseismic coupling in the CVWP. For each simulation, the long-term ISC is computed at each point inside the CVWP using equation 21 **(see Methods A7)** and then averaged spatially across the CVWP. Blue circles and stars correspond to simulations with D_c and σ_n contrast, respectively. Most values are higher than 0.95, implying that in the long term, some barriers can display high ISC.

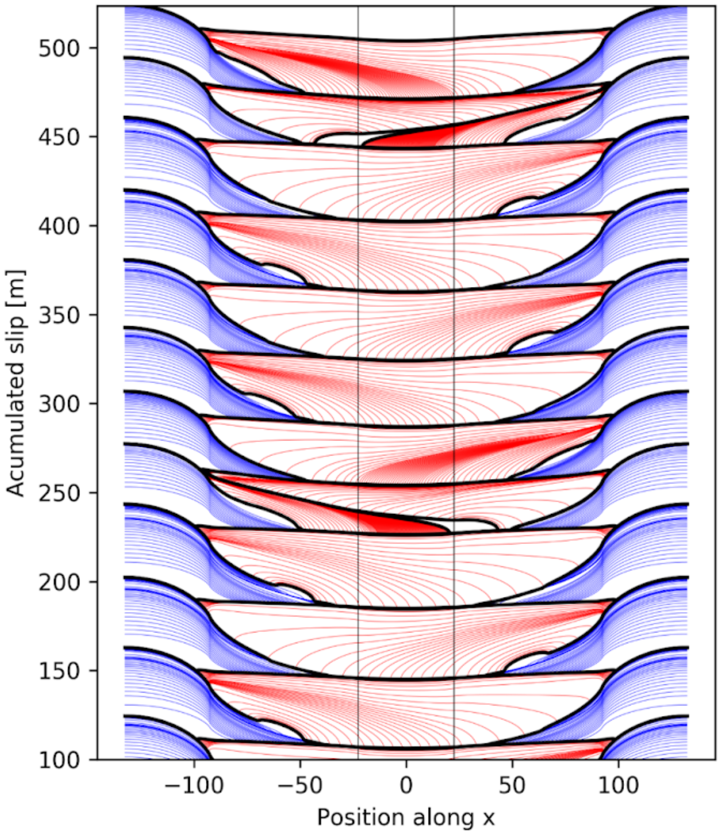

Figure Extended data 4: Reference seismic cycle simulation. Cumulative slip profiles along the fault during interseismic periods (blue, every 2 years) and during earthquakes (red, every 5 seconds); Black lines depict the start and ending of earthquakes. Reference model with uniform $D_c = 0.1\ m$ and $\sigma_n = 95\ MPa$ (there is a small increase of a in a 45 km-long CVWP). **b)** A model with very high $\sigma_n = 220\ MPa$ in a 60 km-long CVWP.

Slip behavior of velocity-weakening barriers

Diego Molina-Ormazabal [1,2], Jean-Paul Ampuero [3], Andrés Tassara [1,2]

1 Departamento Ciencias de la Tierra, Facultad de Ciencias Químicas, Universidad de Concepción, Concepción, Chile,
2 Millennium Nucleus The Seismic Cycle Along Subduction Zones CYCLO, Valdivia, Chile,
3 Université Côte d'Azur, IRD, CNRS, Observatoire de la Côte d'Azur, Géoazur, Sophia Antipolis, France,

Supplementary material

Contents

Predicting barrier efficiency λ

While equation 17 needs to be computed from model outputs, a posteriori, here we propose an a priori estimator of λ based on model inputs. We develop scaling relationships between asperity stress drop ($\Delta\tau_a$) and fault input parameters, σ_n , D_c and L_B. For each simulation, we compute the mean stress drop across the asperity for all earthquakes halting at the barrier or breaking it entirely. For a given set of simulations with fixed D_c (or σ_n) but varying L_B, we estimate the asperity stress drop ($\Delta\tau_{am}$) averaged among all differents L_B cases. We find an almost linear relation between $\Delta\tau_{am}$ and D_c (or σ_n) **[Fig. S1, left panel]**, with best-fitting relations of the following form:

$$\Delta\widehat{\tau}_{am} = a_1 + a_2 \times D_c \quad \text{and} \quad \Delta\widehat{\tau}_{am} = b_1 + b_2 \times \sigma_n \tag{22}$$

where a_1, a_2 , b_1 and b_2 are constants. Similarly, we derive a scaling relation for the barrier stress drop ($\Delta\tau_b$).

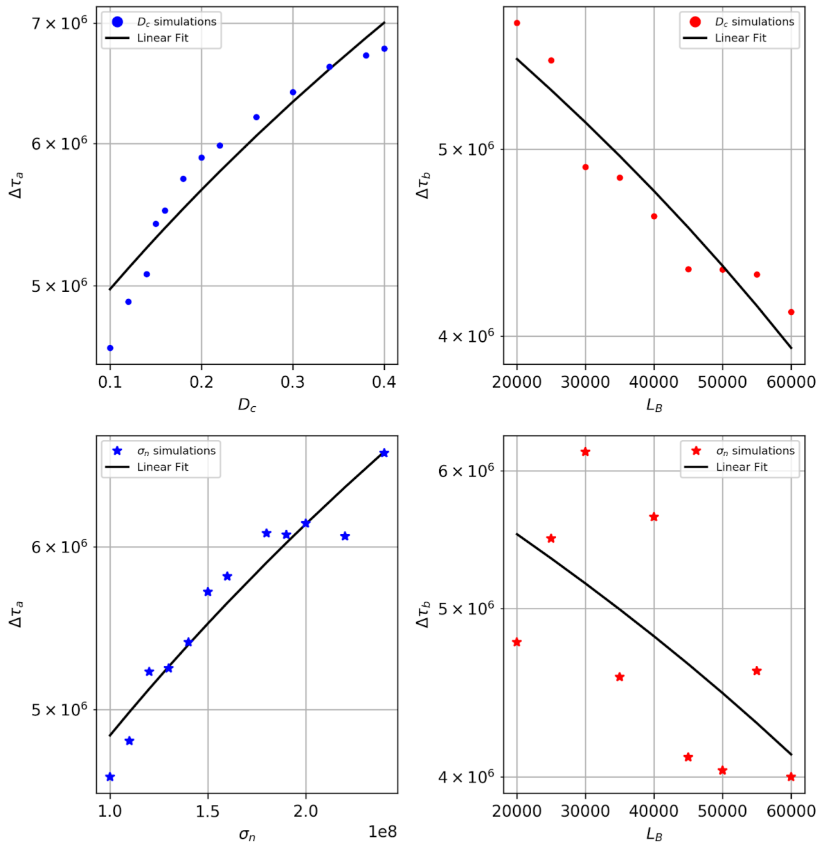

Figure S1: Stress drop dependency with D_c, σ_n or barrier length LB observed from the earthquake simulations. Left panels: Blue dots and stars depict representative asperity stress drop $\Delta\tau_{am}$ values as a function of frictional parameters D_c and σ_n respectively. The black solid line represents a linear polynomial used to fit the values, which allows us to obtain a scaling relation between $\Delta\tau_{am}$ and D_c o σ_n **(equation 22)**. Right panels: Red dots and stars display average barrier stress drop $\Delta\tau_{bm}$ depending on barrier length (L_B) **(equation 23).** The black solid line fits the values, showing an inverse relation between barrier stress drop and its length. These linear fits provide another scaling relation used to predict the barrier efficiency λ.

For simulations with the same barrier length L_B, we take the mean stress drop across the central VW patch for each earthquake, then average among all the events in the simulation set with variable D_c (or σ_n) to obtain a mean barrier stress drop ($\Delta\tau_{bm}$). We find an inverse relation between $\Delta\tau_{bm}$ and L_B, which is more clear in the set with variable D_c **[Fig. S1, right panel]**, with best-fitting relations of the form:

$$\Delta\widehat{\tau}_{bm} = a_3 + a_4 \times L_b \text{ and } \Delta\widehat{\tau}_{bm} = b_3 + b_4 \times L_b \tag{23}$$

for the variable D_c and variable σ_n sets, respectively, where a_3, a_4, b_3 and b_4 are constants.

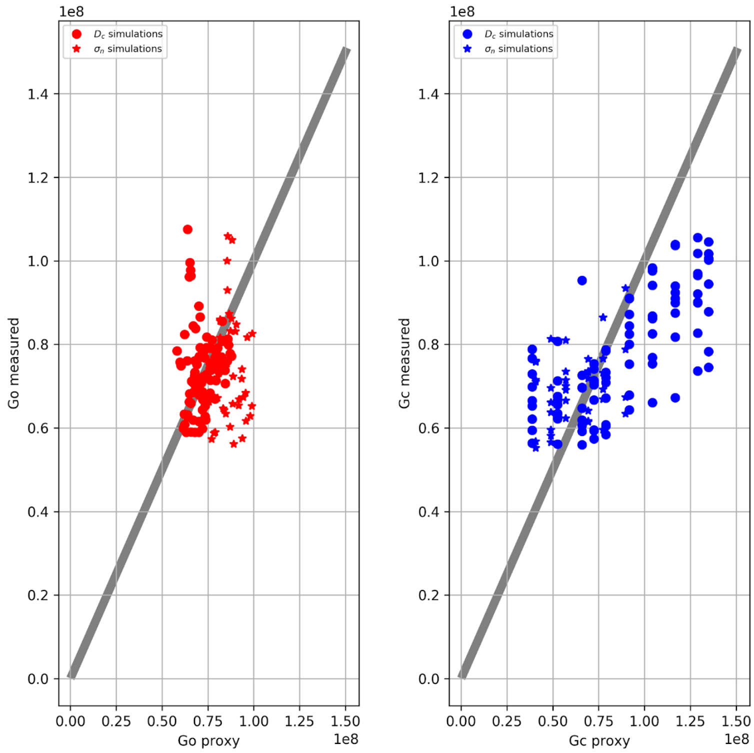

Figure S2: G_o and G_c mean values from simulations (originally used to estimate λ, Methods A3) compared with G_{cp} and G_{1opx} proxies mean values calculated considering stress drop dependency with D_c, σ_n and barrier length L_B [Figure S1]. Left panel: Red stars and circles are estimations for $G_{1\,opx}$ computed for a given value of L_B and D_c (or σ_n) considering stress drop dependency shown in Figure S1 and equation 10 (this work). Then it is compared with the mean Go (used to estimate λ), which is displayed in the y-axis. Right panel: Blue circles (or blue stars) represent G_{cp} (Rubin-Ampuero 2005, **equation 24**) considering the same values of D_c (or σ_n). Then the values are compared with the original G_c average values coming from the simulations (see Methods A4). Gray solid line is the straight line with slope 1, shown for reference. These Gc and Go proxies together with the stress drop predictions **(Fig. S1, Fig. S2)** are finally used to obtain a predicted λ_p (**Fig. S3**)

These scaling relations are then used in equations 10 to estimate G_{oi} for each simulation (see Methods). Then, the proxy predicted for the asperity static energy release rate is called G_{1opx}.

To estimate the fracture energy associated to rate-and-state friction, we adopt the estimate derived by Rubin and Ampuero (2005):

$$G_{cp} = \frac{bD_c\sigma_n[ln(V\theta/D_c)]^2}{2} \qquad (24)$$

In particular, in this expression G_c is proportional to the product $D_c\sigma_n$ of the two fault parameters varied in our simulations. Both, G_{1opx} and G_{cp} are displayed on figure S2.

Finally, the predicted λ_p constrained by our proxies is

$$\lambda_p = \frac{G_c}{G_{1opx}}^{m} T^n \qquad (25)$$

In Figure S3 it can be noted that λ_p is able to reproduce the main tendencies of the original barrier efficiency index derived from our simulations (measured λ).

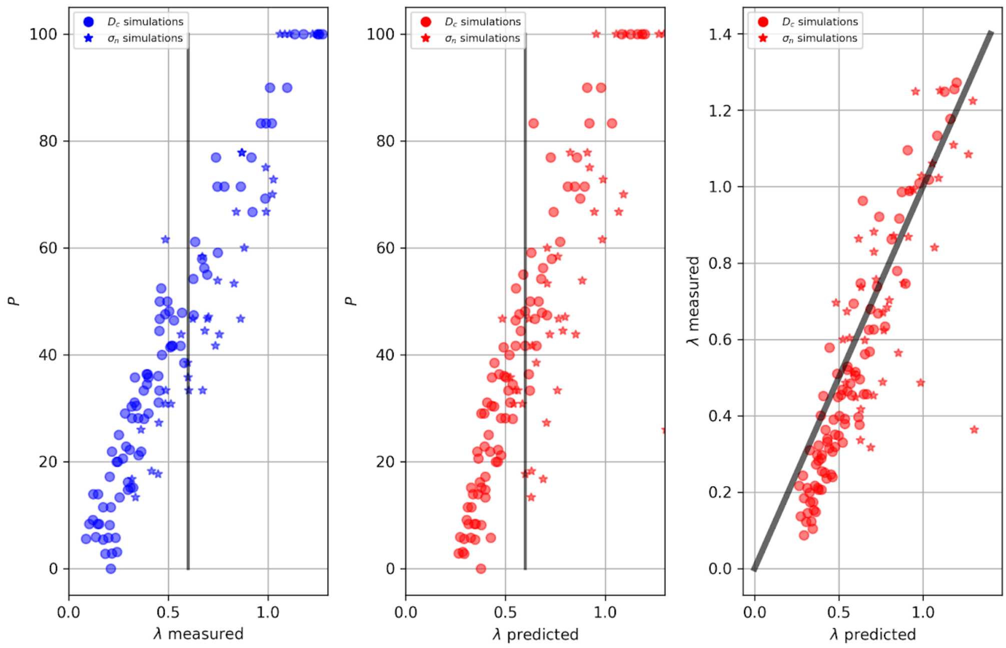

Figure S3: Measured and predicted λ compared with the probability P (Percentage of events breaking the barrier). Left: Blue circles and stars represent estimations of barrier efficiency derived from simulations where D_c and σ_n have been varied respectively [Figure 4c]. **Middle**: predicted values of λ obtained from G_c, G_o proxies **(** $G_{1opx}G_{cp}$, **Figure S2,)** and stress drop scaling **(equations 22, 23)** with frictional and geometrical parameters (D_c , σ_n circles and stars respectively). Red represents λ_p **(equation 25)**. Vertical gray line shows the threshold of temporary or permanent barriers. For $\lambda < 0.3$ the probability of having permanent barrier increases and for $\lambda > 1$ the probability of having temporary barrier increases too. **Right:** Measured λ values [y-axis] as a function of predicted λ_p [x-axis]. Solid gray line displays the slope 1 reflecting 1 to 1 correlation.

Estimating the efficiency of natural barriers

Natural seismic barriers can be categorized through the efficiency barrier parameter λ derived in this work (equation 17) by devising estimates of the quantities involved (G_c, G_{oi} and $\Delta\tau$) based on observable quantities. While the simulations conducted here assumed rate-and-state friction, fault friction at the natural scale is expected to involve additional weakening processes. In the absence of a universal friction law for faults, following Weng and Ampuero (2020), we consider an empirical relation between G_c and final slip S of the form $G_c \sim BS^n$, where $B \approx 3$ and $n \approx 0.7$ are constants constrained by seismological observations. We estimate the asperity energy as $G_{oi} = \frac{\pi L_A \Delta\tau_A{}^2}{4\mu}$ where $\Delta\tau_A \sim \mu S_A / L_A$ is the stress drop on the asperity, S_A its slip and L_A its length. Using these relations and equation 17, we define a new barrier efficiency proxy:

$$\lambda' = \left[\frac{4 L_A B S_B^n}{\pi \mu S_A^2}\right]^m \left[\frac{S_B L_A}{S_A L_B}\right]^n$$

where L_A and L_B are the asperity and barrier lengths, respectively, and S_B and S_A are the final averaged slip on the barrier and asperity, respectively.

As an example, we evaluate the proxy λ' for the Chilean margin around the southern end of the rupture area of the 2010 Maule earthquake. We estimate the length of the Maule South Segment ($L_A = 124\ km$) and the Arauco barrier ($L_B = 50\ km$) and the depth-averaged slip deficit from fault locking models based on geodetic data **(Figure S4; Molina et al., 2021; Moreno et al., 2010)**. The slip deficit is obtained by multiplying the slip deficit rate **(Fig. S4 a)** and the time elapsed since the last big earthquake in 1835, and is then averaged across the seismogenic depth **(Fig. S4 b)**. The resulting values are $S_B = 5.6\ m$ and $S_A = 6.8\ m$, which yield $\lambda' = 0.23$, categorizing the Arauco peninsula as a permanent barrier based on Fig 4c.

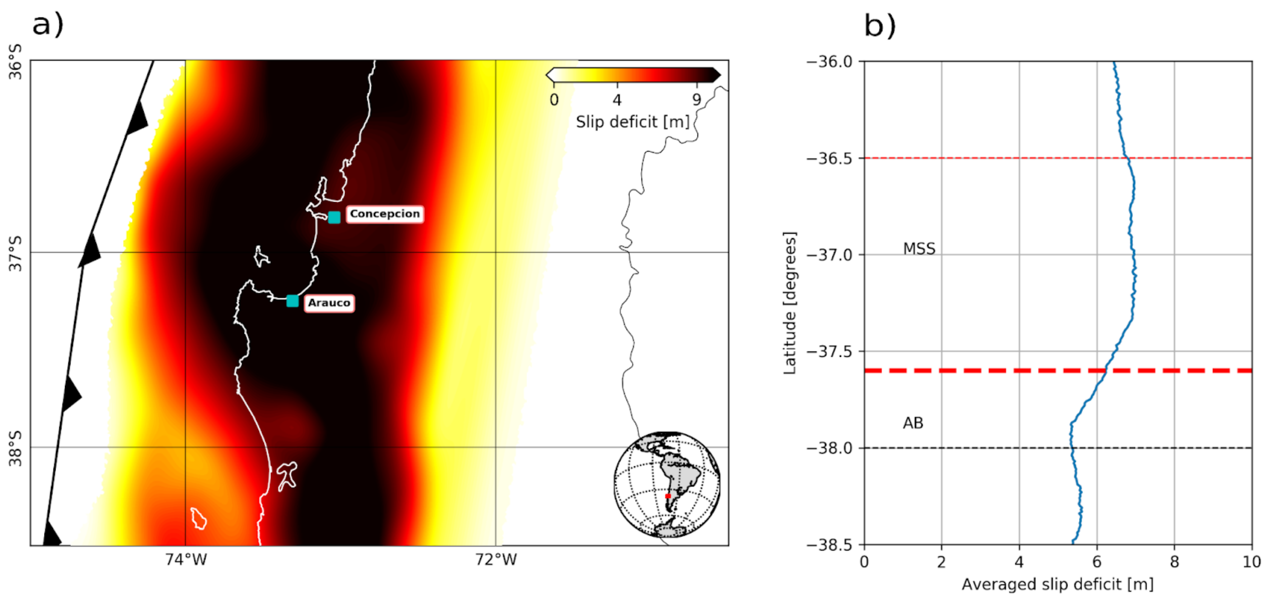

Figure S4: Slip deficit for the Maule earthquake area. a) Slip deficit in 2010 over the rupture area of the 2010 Maule earthquake considering 175 years of accumulation period since the last big earthquake in the region in 1835. b) Along-strike distribution of depth-averaged slip deficit (blue curve). Dashed red lines indicate the boundaries of the Maule South Segment (MSS). The thicker red line and black line indicate the boundaries of the Arauco barrier (AB).